

Model of commensurate harmonic oscillators with SU(2) coupling interactions: Analogous observation in laser transverse modes

Y. C. Lin,¹ T. H. Lu,² K. F. Huang,¹ and Y. F. Chen^{1,*}

¹*Department of Electrophysics, National Chiao Tung University, Hsinchu, Taiwan*

²*Department of Physics, National Taiwan Normal University, Taipei, Taiwan*

(Received 10 February 2012; published 24 April 2012)

We theoretically explore the eigenstates of a coupled $p:q$ commensurate harmonic oscillator with SU(2) coupling interactions under the canonical transformation. The spatial patterns of the high-order eigenstates are found to be markedly localized on Lissajous figures from single to multiple periodic orbits. Controlling the pumping size in large-Fresnel-number degenerate cavities, we have experimentally observed the laser transverse modes that display the wave patterns to be analogous to the derived eigenstates.

DOI: [10.1103/PhysRevE.85.046217](https://doi.org/10.1103/PhysRevE.85.046217)

PACS number(s): 05.45.-a, 03.65.Fd, 03.65.Ge, 03.65.Vf

I. INTRODUCTION

For the past few decades, models developed from quantum mechanics have been employed progressively to explore the emergent phenomena in numerous different branches of physics because they can be interpreted with the same theoretical forms as quantum formulas [1–5]. One of the most profound similarities is that the electromagnetic wave equation in paraxial approximation is isomorphous to the Schrödinger equation [6–9]. Consequently, the electromagnetic radiation modes in the optical resonator or waveguide are analogs of the wave functions of a quantum system [10–12]. The tight connection between the paraxial beam propagation and quantum mechanics has been extensively exploited to study wave chaos phenomena [11,13,14], disorder induced wave localization [15], semiclassical physics [16,17], and transient dynamics of quantum states [18–20].

The coupled harmonic oscillators (HOs) have been employed successfully to explore the hydrogen atom problem [21], charged particles in external field [22,23], states of deformed nucleus in the Nilson model [24], shell effects in nuclei and metallic clusters [25], and orbital magnetism in quantum dots [26]. More recently, the isotropic HOs with SU(2) coupling interactions have been used to investigate the generation and evolution of quantum vortex states [27] and the transformation geometry between Lissajous and trochoidal orbits [28]. It has been shown [29,30] that the commensurate HOs can be mapped into the isotropic HOs via the canonical transformation. Although the isotropic HOs with SU(2) coupling interactions have been verified to be a striking analytical model, the quantum states of canonically mapped commensurate HOs with SU(2) coupling interactions have not been thoroughly explored yet.

In this work we start from a coupled $p:q$ commensurate HO with canonical transformation to develop a quantum mechanical model with SU(2) coupling interactions. We explore the eigenstates and find that the high-order spatial patterns are noticeably concentrated on Lissajous figures from single to multiple periodic orbits. In an earlier work [12], the three-dimensional (3D) coherent lasing modes with transverse patterns corresponding to single Lissajous figures have been

methodically generated in degenerate cavities with a large off-axis tightly focused pumping scheme. Here we intriguingly verified that the 3D coherent lasing waves can be manipulated to form more intricate transverse patterns corresponding to multiple Lissajous orbits as found in the quantum eigenstates of the developed model. The number of Lissajous orbits in the lasing transverse pattern is experimentally confirmed to be proportional to the pumping spot size. More importantly, the role of the phase factor introduced by the SU(2) coupling interactions can be nicely manifested from the propagating property of the lasing modes. We expect that the findings of controlling lasing transverse modes with spatial patterns to be related to quantum states could open new attractive issues in quantum physics and optical pattern formations.

II. THEORETICAL MODEL

The general form of a $p:q$ two-dimensional (2D) commensurate anisotropic HO comprising a weak coupling term can be modeled as

$$\hat{H} = \hat{H}_0 + \hat{H}_c, \quad (1)$$

where \hat{H}_c signifies the coupling characterized by a vibration-rotational mechanism and the detail will be provided later. With dimensionless spatial operators \hat{x} and \hat{y} , the Hamiltonian of the $p:q$ commensurate anisotropic HO \hat{H}_0 can be given as [29]

$$\hat{H}_0 = \frac{1}{2}(\hat{p}_x^2 + \hat{p}_y^2 + \omega_1^2 \hat{x}^2 + \omega_2^2 \hat{y}^2), \quad (2)$$

where $\omega_1 = q\omega$ and $\omega_2 = p\omega$, ω is a common factor of the oscillation frequencies ω_1 and ω_2 , and q and p are integers. In terms of the ladder operators, the Hamiltonian (2) becomes

$$\hat{H}_0 = \omega' \left[\frac{1}{p} \left(\hat{a}_1^\dagger \hat{a}_1 + \frac{1}{2} \right) + \frac{1}{q} \left(\hat{a}_2^\dagger \hat{a}_2 + \frac{1}{2} \right) \right], \quad (3)$$

where $\omega' = \omega pq$, $\hat{a}_1 = (q\omega\hat{x} + i\hat{p}_x)/\sqrt{2q\omega}$, $\hat{a}_2 = (p\omega\hat{y} + i\hat{p}_y)/\sqrt{2p\omega}$, $\hat{a}_1^\dagger = (q\omega\hat{x} - i\hat{p}_x)/\sqrt{2q\omega}$, and $\hat{a}_2^\dagger = (p\omega\hat{y} - i\hat{p}_y)/\sqrt{2p\omega}$. The eigenstates of the commensurate anisotropic HO in Eq. (3) are $|n_1 p + \lambda_1, n_2 q + \lambda_2\rangle_{\hat{H}_0}$ as has been shown by Louck *et al.* [29], where (n_1, n_2) are arbitrary non-negative integers, and (λ_1, λ_2) are constants that $\lambda_1 = 0, 1, \dots, p-1$ and $\lambda_2 = 0, 1, \dots, q-1$. The normalized spatial

*yfchen@cc.nctu.edu.tw

representation is the well-known Hermite-Gaussian states [32]

$$\begin{aligned} & \langle x, y | n_1 p + \lambda_1, n_2 q + \lambda_2 \rangle_{\hat{H}_0} \\ &= [2^{n_1 p + n_2 q + \lambda_1 + \lambda_2} (n_1 p + \lambda_1)! (n_2 q + \lambda_2)! \pi]^{-1/2} \\ & \times e^{-(x^2 + y^2)/2} H_{n_1 p + \lambda_1}(x) H_{n_2 q + \lambda_2}(y), \end{aligned} \quad (4)$$

where $H_n(\cdot)$ is the Hermite polynomial of order n . It reveals the fact that the eigenstates have been divided into pq different subsets of states and the degeneracy holds when $n_1 + n_2$ is a constant N for fixed (λ_1, λ_2) corresponding to the eigenvalues $E = \omega'[(n_1 + n_2) + 1/2p + 1/2q + \lambda_1/p + \lambda_2/q]$ of Eq. (3). For a particular case $(p, q) = (1, 1)$ of the isotropic HO, it is evident that Eq. (3) implies $\hat{H}_0 = \omega'[2\hat{J} + 1]$, where \hat{J} is the Casimir operator associated with the SU(2) Lie algebra and the corresponding generators derived by Schwinger [32] are

$$\begin{aligned} \hat{J}_1 &= (\hat{a}_1^\dagger \hat{a}_2 + \hat{a}_2^\dagger \hat{a}_1)/2, & \hat{J}_2 &= (\hat{a}_1^\dagger \hat{a}_2 - \hat{a}_2^\dagger \hat{a}_1)/2i, \\ \hat{J}_3 &= (\hat{a}_1^\dagger \hat{a}_1 - \hat{a}_2^\dagger \hat{a}_2)/2. \end{aligned} \quad (5)$$

The operators \hat{J}_i follow the angular momentum commutation relation $[\hat{J}_i, \hat{J}_j] = i\hbar \varepsilon_{ijk} \hat{J}_k$ [32], where the Levi-Civita tensor ε_{ijk} equals $+1$ (-1) if (i, j, k) is an even (odd) permutation, and zero otherwise.

With the nonbijective canonical transformation, the commensurate anisotropic HO can be mapped onto an isotropic one in a degenerate eigenspace [29]. The mapping suggests Schwinger's development of SU(2) symmetry represented by the canonically transformed ladder operators and leads to the analytical solutions to the Hamiltonian in Eq. (3). Therefore, under the canonical transformation, the Hamiltonian in Eq. (3) can be transformed into

$$\hat{H}_0 = \omega'[(\tilde{a}_1^\dagger \tilde{a}_1 + \frac{1}{2}) + (\tilde{a}_2^\dagger \tilde{a}_2 + \frac{1}{2})], \quad (6)$$

where \tilde{a}_i and \tilde{a}_i^\dagger ($i = 1, 2$) are the canonically transformed ladder operators which bear the relations [29]

$$\begin{aligned} \tilde{a}_i^\dagger &= \sqrt{\frac{1}{\xi_i}} (\hat{n}_i - \lambda_i) [\hat{n}_i (\hat{n}_i - 1) \cdots (\hat{n}_i - \xi_i + 1)]^{-1/2} (\hat{a}_i^\dagger)^{\xi_i}, \\ \tilde{a}_i &= \sqrt{\frac{1}{\xi_i}} (\hat{n}_i - \lambda_i) [\hat{n}_i (\hat{n}_i - 1) \cdots (\hat{n}_i - \xi_i + 1)]^{-1/2} (\hat{a}_i)^{\xi_i}, \end{aligned} \quad (7)$$

with number operator $\hat{n}_i = \hat{a}_i^\dagger \hat{a}_i$ and $(\xi_1, \xi_2) = (p, q)$. The operation of the ladder operators on particular eigenstates for fixed (λ_1, λ_2) , for instance, are $\tilde{a}_1^\dagger |n_1 p + \lambda_1, n_2 q + \lambda_2\rangle_{\hat{H}_0} = \sqrt{n_1 + 1} |(n_1 + 1)p + \lambda_1, n_2 q + \lambda_2\rangle_{\hat{H}_0}$ and $\tilde{a}_1 |n_1 p + \lambda_1, n_2 q + \lambda_2\rangle_{\hat{H}_0} = \sqrt{n_1} |(n_1 - 1)p + \lambda_1, n_2 q + \lambda_2\rangle_{\hat{H}_0}$. Obviously,

Eq. (6) is converted into the same form as the isotropic HO when the degeneracy can exist for $n_1 + n_2 = N$ according to the eigenvalue $E = \omega'(n_1 + n_2 + 1)$ to the Hamiltonian \hat{H} . The generators of the SU(2) symmetry group can be rewritten in a way that makes them the generators responsible for the anisotropic HO under consideration:

$$\begin{aligned} \tilde{J}_1 &= (\tilde{a}_1^\dagger \tilde{a}_2 + \tilde{a}_2^\dagger \tilde{a}_1)/2, & \tilde{J}_2 &= (\tilde{a}_1^\dagger \tilde{a}_2 - \tilde{a}_2^\dagger \tilde{a}_1)/2i, \\ \tilde{J}_3 &= (\tilde{a}_1^\dagger \tilde{a}_1 - \tilde{a}_2^\dagger \tilde{a}_2)/2. \end{aligned} \quad (8)$$

The operators also satisfy the Lie commutation relation. Particularly, $\tilde{J}_1 = \hat{J}_1$, $\tilde{J}_2 = \hat{J}_2$, and $\tilde{J}_3 = \hat{J}_3$ for the special case of the isotropic HO with $(p, q) = (1, 1)$.

Let us now return to our formal considerations of the coupled anisotropic HO of the Hamiltonian given in Eq. (1). The coupling term \hat{H}_c is introduced as an SU(2) coupling interaction [27,28], which can be modeled as

$$\hat{H} = \hat{H}_0 + \hat{H}_c = \hat{H}_0 + (A\tilde{J}_1 + B\tilde{J}_2 + C\tilde{J}_3), \quad (9)$$

where A , B , and C are constants indicating the coupling parameters with the assumption A , B , and $C \leq \omega'$ for weak coupling. We would like to remark that, in view of the case $(p, q) = (1, 1)$ for the coupled isotropic HO, the wave functions have been demonstrated previously on a group theory level via the SU(2) transformation [28,31]. Likewise, it enables us to derive the wave functions by employing the transformation of the SU(2) symmetry group.

Now consider our problem of the Hamiltonian in Eq. (9); that is, find the eigenstates to the commensurate coupled HO. Under the SU(2) transformation, the eigenstates to the Hamiltonian in Eq. (9) can be given as

$$\begin{aligned} & |n_1 p + \lambda_1, n_2 q + \lambda_2\rangle_{\hat{H}} \\ &= \hat{U} |n_1 p + \lambda_1, n_2 q + \lambda_2\rangle_{\hat{H}_0} \\ &= e^{-i\alpha \tilde{J}_3} e^{-i\beta \tilde{J}_2} |n_1 p + \lambda_1, n_2 q + \lambda_2\rangle_{\hat{H}_0}, \end{aligned} \quad (10)$$

where $\hat{U} = e^{-i\alpha \tilde{J}_3} e^{-i\beta \tilde{J}_2}$ is the unitary operator, $\alpha = -\tan^{-1}(B/A)$, and $\beta = -\tan^{-1}(\sqrt{A^2 + B^2}/C)$. The Hamiltonian \hat{H} can be diagonalized into $\hat{H}' = \hat{U}^{-1} \hat{H} \hat{U} = \hat{H}_0 + \sqrt{A^2 + B^2 + C^2} \tilde{J}_3$. Therefore, with the operation on eigenstates $|n_1 p + \lambda_1, n_2 q + \lambda_2\rangle_{\hat{H}_0}$, eigenvalues to \hat{H} can be directly achieved as $E' = \omega'(n_1 + n_2 + 1) + \sqrt{A^2 + B^2 + C^2}(n_1 - n_2)/2$, where nearly degenerate occurs for $n_1 + n_2 = N$, where N is a constant. Consequently, the eigenstates to the Hamiltonian \hat{H} can be obtained in terms of the Wigner d coefficient [33]:

$$|n_1 p + \lambda_1, n_2 q + \lambda_2\rangle_{\hat{H}} = e^{iN\alpha/2} \left(\sum_{m_1=0}^N e^{-im_1\alpha} d_{m_1-N/2, n_1-N/2}^{N/2}(\beta) |m_1 p + \lambda_1, m_2 q + \lambda_2\rangle_{\hat{H}_0} \right), \quad (11)$$

where

$$d_{m_1-N/2, n_1-N/2}^{N/2}(\beta) = \sqrt{m_1!(N-m_1)!n_1!(N-n_1)!} \sum_{v=\max[0, m_1-n_1]}^{\min[N-n_1, m_1]} \frac{(-1)^v [\cos(\beta/2)]^{n_1+m_1-2v} [\sin(\beta/2)]^{n_2-m_1+2v}}{v!(N-n_1-v)!(m_1-v)!(n_1-m_1+v)!}, \quad (12)$$

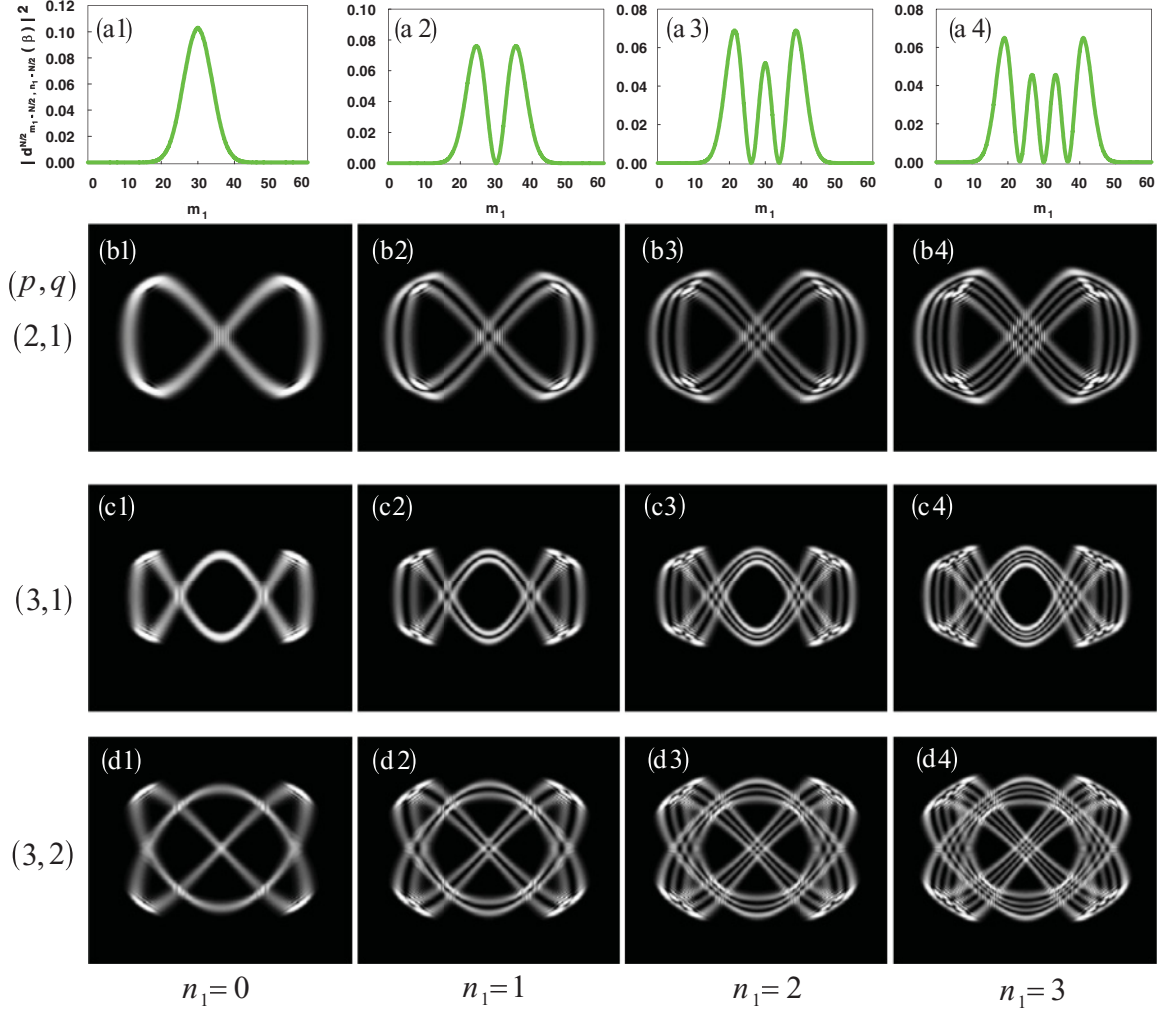


FIG. 1. (Color online) (a1)–(a4) Numerical simulations of Wigner d coefficient $|d_{m_1-N/2, n_1-N/2}^{N/2}(\beta)|^2$ with respect to m_1 for various n_1 . (b1)–(d4) Numerical wave patterns for the intensities of eigenstates $|n_1 p + \lambda_1, n_2 q + \lambda_2\rangle_{\hat{H}}$. See text for a detailed description of the parameters.

and $m_1 + m_2 = N$. Evidently, eigenstates $|n_1 p + \lambda_1, n_2 q + \lambda_2\rangle_{\hat{H}}$ can be expressed as a linear superposition of the set of $|m_1 p + \lambda_1, m_2 q + \lambda_2\rangle_{\hat{H}_0}$. Figures 1(a1)–1(a4) show distributions of the Wigner d coefficient $|d_{m_1-N/2, n_1-N/2}^{N/2}(\beta)|^2$ with respect to m_1 for $n_1 = 0-3$, $n_1 + n_2 = N$, $N = 60$, and $\beta = \pi/2$, which reveal the composition of $|n_1 p + \lambda_1, n_2 q + \lambda_2\rangle_{\hat{H}}$ with eigenstates $|m_1 p + \lambda_1, m_2 q + \lambda_2\rangle_{\hat{H}_0}$ of different orders. Figures 1(b1)–1(b4), 1(c1)–1(c4), and 1(d1)–1(d4) illustrate the corresponding eigenstates $|n_1 p + \lambda_1, n_2 q + \lambda_2\rangle_{\hat{H}}$ with $(p, q) = (2, 1)$, $(p, q) = (3, 1)$, and $(p, q) = (3, 2)$, respectively, and all with $(\lambda_1, \lambda_2) = (0, 0)$, $(\alpha, \beta) = (\pi/2, \pi/2)$, $n_1 + n_2 = N$, and $N = 60$.

Note that it is valid for us to choose a specific eigenspace of $(\lambda_1, \lambda_2) = (0, 0)$ since, in the classical limit (N large enough), [34] has confirmed that the choice of the eigenspace does not affect the final results. Therefore, parameters (λ_1, λ_2) are set to be $(0, 0)$ in the following discussions. Moreover, (α, β) are chosen for specific parameters. α signifies an additional phase shift between the two HOs in x and y directions, and β corresponds to the coupling strength arising from \hat{H}_c . The

distribution $|d_{m_1-N/2, n_1-N/2}^{N/2}(\beta)|^2$ shown in Figs. 2(a1)–2(a8) are varied with β , which indicates different composition of the corresponding eigenstates $|n_1 p, n_2 q\rangle_{\hat{H}}$ as that depicted in Figs. 2(b1)–2(b8) with $(p, q) = (2, 1)$, $\alpha = \pi/2$, $n_1 = 1$, and $N = 60$. For $\beta = 0$ and $\beta = \pi$, the eigenstates can be seen to project precisely onto particular eigenstates $|p, q(N-1)\rangle_{\hat{H}_0}$ and $|p(N-1), q\rangle_{\hat{H}_0}$, respectively. While β is determined, the conversion of α can be illustrated as shown in Figs. 3(a1)–3(a5) with $n_1 = 1$, $\beta = 0.4\pi$, and $N = 60$, and in Figs. 3(b1)–3(b5) with $n_1 = 3$, $\beta = 0.74\pi$, and $N = 60$. The morphologies transform since different relative phases are introduced into the superposition of states $|n_1 p, n_2 q\rangle_{\hat{H}}$ with the set of states $|m_1 p, m_2 q\rangle_{\hat{H}_0}$.

Theoretical results disclose intriguing geometric patterns localized on an ensemble of periodic Lissajous orbits, which suggests a kind of quantum-classical analog. It is evidenced that the number of peaks of $|d_{m_1-N/2, n_1-N/2}^{N/2}(\beta)|^2$ is consistent with the number of Lissajous orbits of $|n_1 p, n_2 q\rangle_{\hat{H}}$ for various n_1 . This fact implies that each orbit of the multi-Lissajous patterns is formed by the superposition of a particular group of the set $|m_1 p, m_2 q\rangle_{\hat{H}_0}$ with distribution centered on the

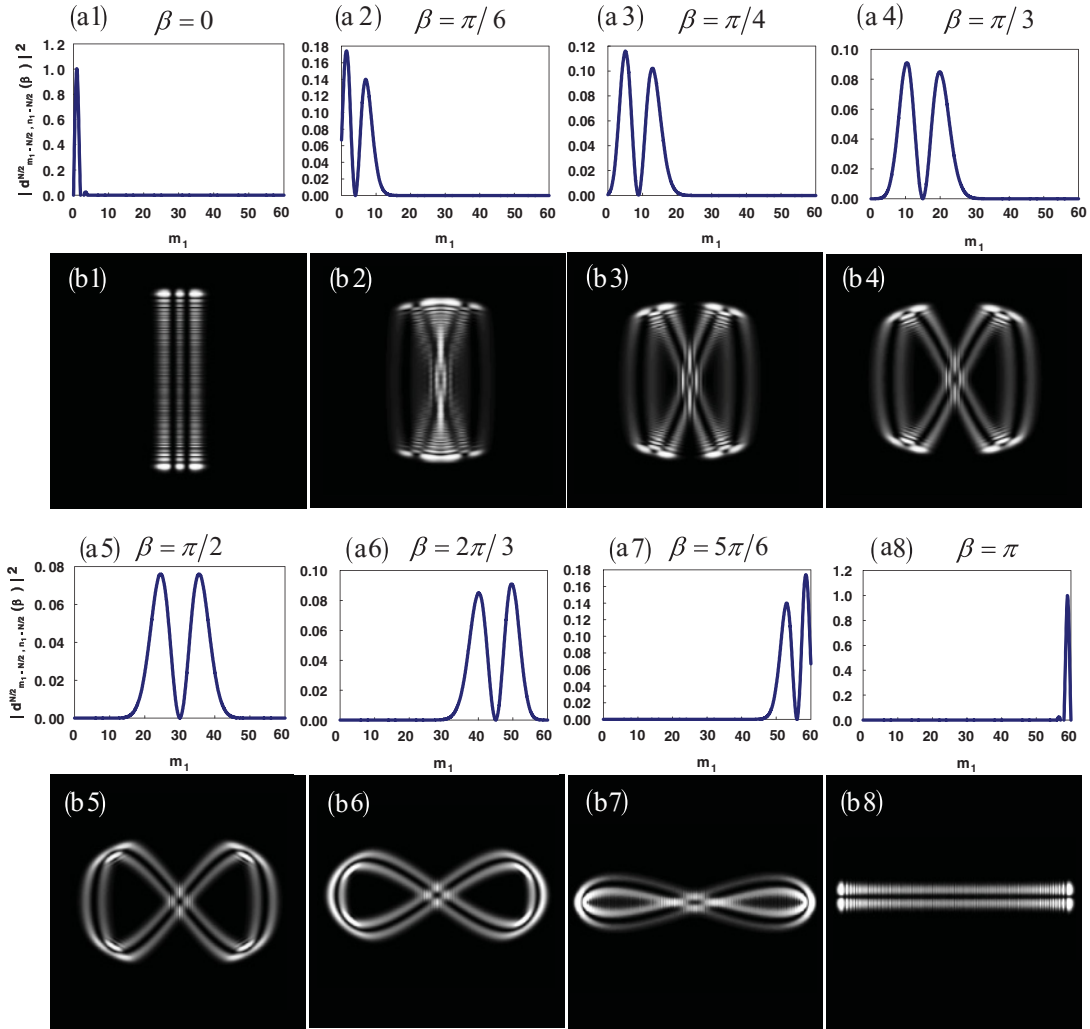


FIG. 2. (Color online) (a1)–(a8) Numerical simulations of Wigner d coefficient $|d_{m_1-N/2, n_1-N/2}^{N/2}(\beta)|^2$ with respect to m_1 for various β . (b1)–(b8) Corresponding numerical wave patterns for the intensities of eigenstates $|n_1 p, n_2 q\rangle_{\hat{H}}$.

corresponding peak of $|d_{m_1-N/2, n_1-N/2}^{N/2}(\beta)|^2$. A relation $l = \min(n_1, n_2) + 1$ can be given, where l denotes the number of

orbits. While the magnitude of $\min(n_1, n_2)$ becomes larger, the related excited states display more complex causticlike

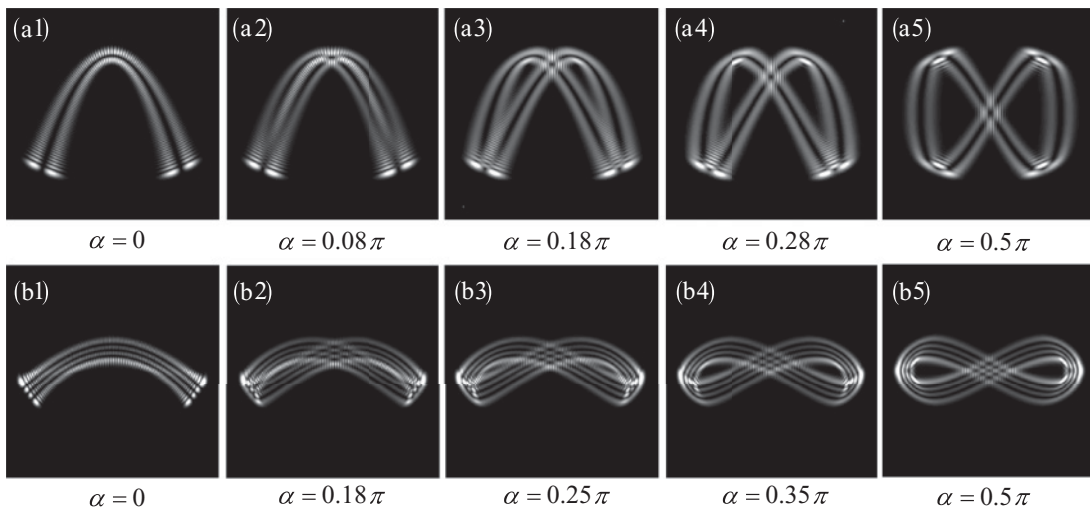


FIG. 3. Numerical wave patterns for the intensities of eigenstates $|n_1 p, n_2 q\rangle_{\hat{H}}$ with respect to varying α . (a1)–(a5) $\beta = 0.4\pi$. (b1)–(b5) $\beta = 0.74\pi$.

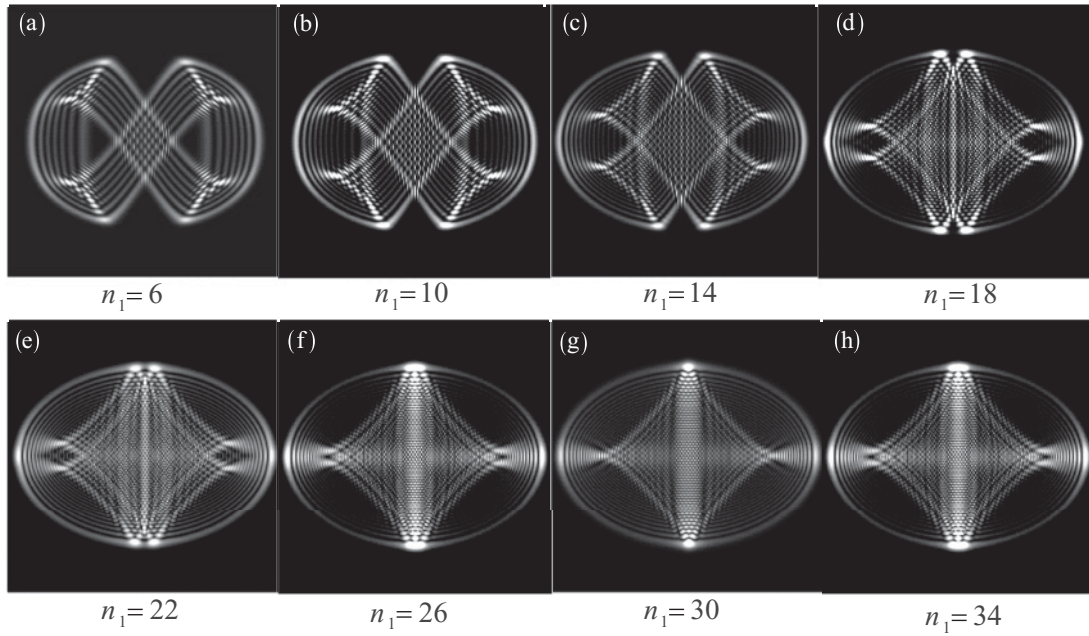


FIG. 4. Numerical wave patterns for higher indices n_1 followed by the case in Figs. 1(b1)–1(b4).

geometric patterns as shown in Fig. 4, followed by the case in Figs. 1(b1) and 1(b2). Additionally, the symmetry is held for $(n_1, n_2) \Leftrightarrow (n_2, n_1)$, e.g., eigenstates of $(n_1, n_2) = (26, 34)$ and $(n_1, n_2) = (34, 26)$ shown in Figs. 4(f) and 4(h) possess identical morphology for equal distribution $|d_{m_1-N/2, n_1-N/2}^{N/2}(\beta)|^2$. Though the same morphology is notified, the eigenstates (n_1, n_2) and (n_2, n_1) are characterized by distinct features of the quantum probability current \vec{J} , where $\vec{J}(x, y) = \text{Im}(\Psi^* \nabla \Psi)$ [33] and $\Psi_{n_1 p, n_2 q}(x, y) = \langle x, y | n_1 p, n_2 q \rangle_{\hat{H}}$. Taking the cases of $(n_1, n_2) = (1, 59)$ and $(n_1, n_2) = (59, 1)$ as an example, it can be seen that the probability current $\vec{J}(x, y)$ flows in counter directions for the two states as depicted in Figs. 5(b) and 5(c). Note that the vector field $\vec{J}(x, y)$ has been normalized to $\vec{J}(x, y)/|\vec{J}(x, y)|$ for observing the detailed structures, and the constants \hbar and particle mass are set to be unity.

Figure 6 further displays the phase structures for the case in Figs. 4(a) and 4(e). The enlarged figures of the box region in Figs. 6(a2) and 6(b2) are presented, respectively, in Figs. 6(a3)

and 6(b3), where the complicated phase distribution indicates promising development in quantum physics such as quantum entanglement and quantum information as long as the quantum states $|n_1 p, n_2 q\rangle_{\hat{H}}$ can be accessibly prepared [35]. As we will see in the following, the correlated optical modes can be successfully generated in an astigmatic large-Fresnel-number laser cavity [31]. The certification is based on the reconciliation between the wave equation for laser transverse modes in the paraxial approximation and the Schrödinger equation for the 2D quantum confined systems [10–12]. Most importantly, Nienhuis *et al.* [10] has clarified high correlation between the quantum operator algebra and manipulation in the laser cavity. Consequently, based on the acts of the quantum operators $e^{-i\alpha \hat{J}_3} e^{-i\beta \hat{J}_2}$ in Eq. (10), we are able to generate the analogous wave patterns by the correlated operation in a laser resonator. The presented research will not be restricted to the theoretical viewpoint of quantum physics and, intriguingly, practical correspondence will be explicitly provided with optical waves.

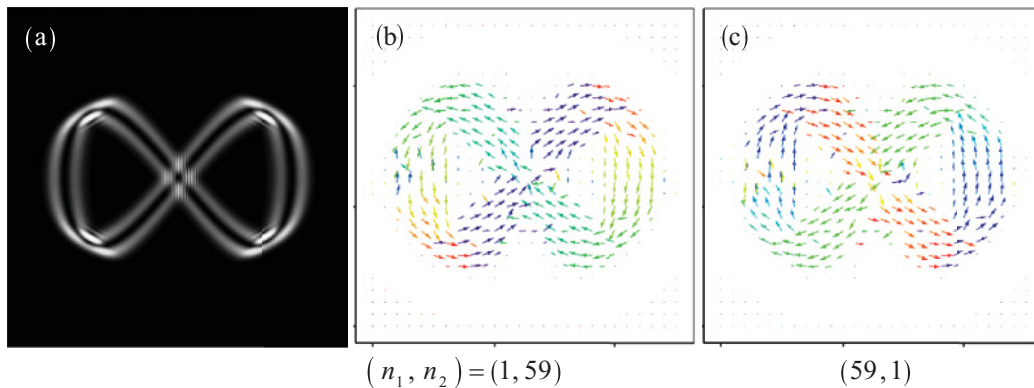


FIG. 5. (Color online) (a) Numerical wave patterns for the intensities of eigenstates $|n_1 p, n_2 q\rangle_{\hat{H}}$ for $(n_1, n_2) = (1, 59)$ and $(n_1, n_2) = (59, 1)$; probability current $\vec{J}(x, y)$ for (b) $(n_1, n_2) = (1, 59)$ and (c) $(n_1, n_2) = (59, 1)$.

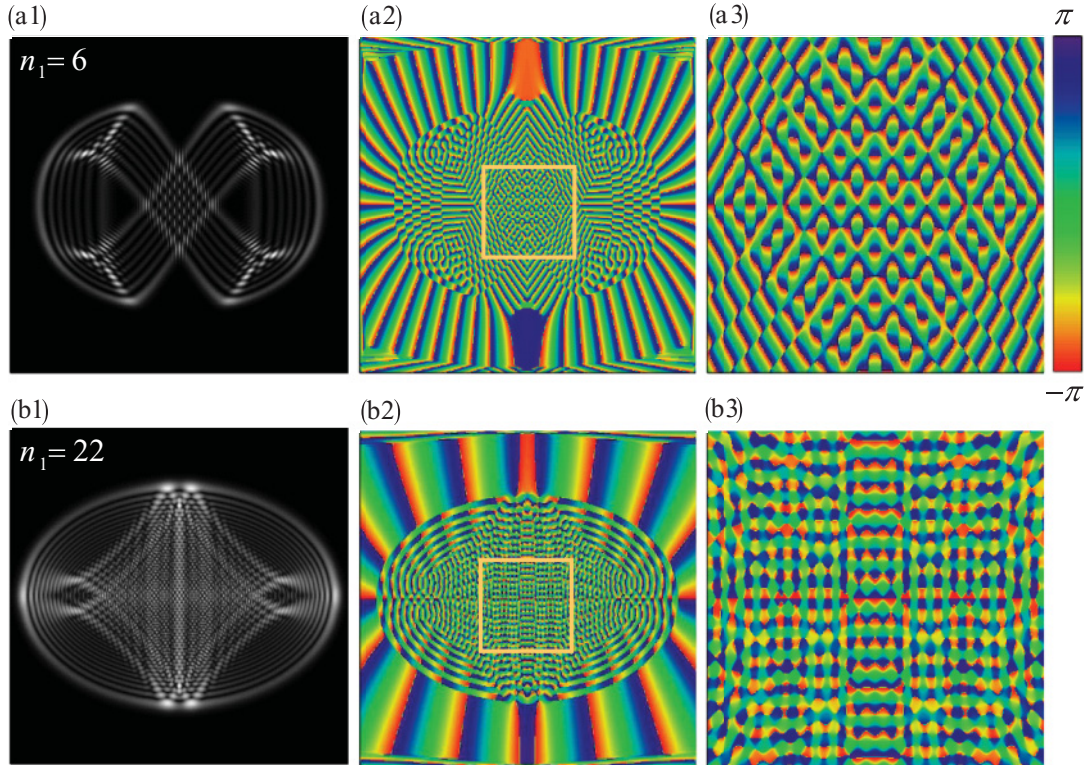


FIG. 6. (Color online) (a1),(b1) Theoretical results in Figs. 4(a) and 4(e). (a2),(b2) Phase distribution of (a1) and (b1), respectively. (a3), (b3) Enlarged figures of the box region in (a2) and (b3), respectively.

III. ANALOGOUS OBSERVATION IN LASER TRANSVERSE MODES

The experiment mainly consists of a laser resonator, a pumping source, and an imaging system as shown in Fig. 7(a). The laser resonator is composed of a spherical mirror and a large-aperture gain medium. The gain medium is an a-cut 2.0-at. % Nd:YVO₄ crystal with a length of 2 mm and a 10 × 10 mm² cross section. Two sides of the crystals are coated for high reflection and antireflection, respectively, at 1064 nm. The radius of curvature of the spherical mirror is $R = 10$ mm

and its reflectivity is 99.7% at 1064 nm. The pump source is a 3 W 808 nm fiber-coupled laser diode with a pump core of 100 μm in radius. A focusing lens with a focal length of 20 mm and 90% coupling efficiency is employed to reimage the pump beam into the crystal.

The length of the present resonator can be set to form various degenerate cavities in which a resonance frequency with a high-order transverse mode is equal to another resonance frequency with fundamental transverse modes [36]. It has been found [12,31] that the lasing modes in degenerate

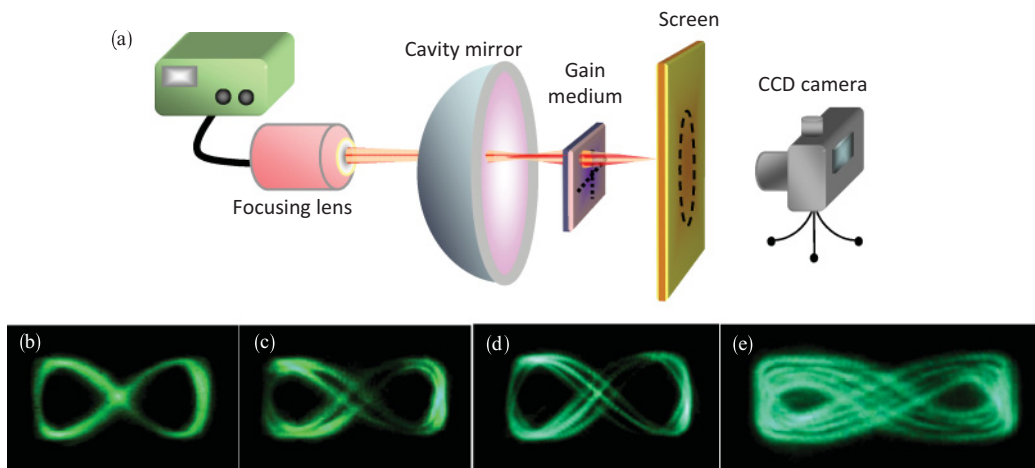


FIG. 7. (Color online) (a) Experimental setup for the generation of laser modes with large off-axis defocusing pumping. (b)–(e) Experimental far-field patterns corresponded to the numerical results in Figs. 1(b1)–1(b4).

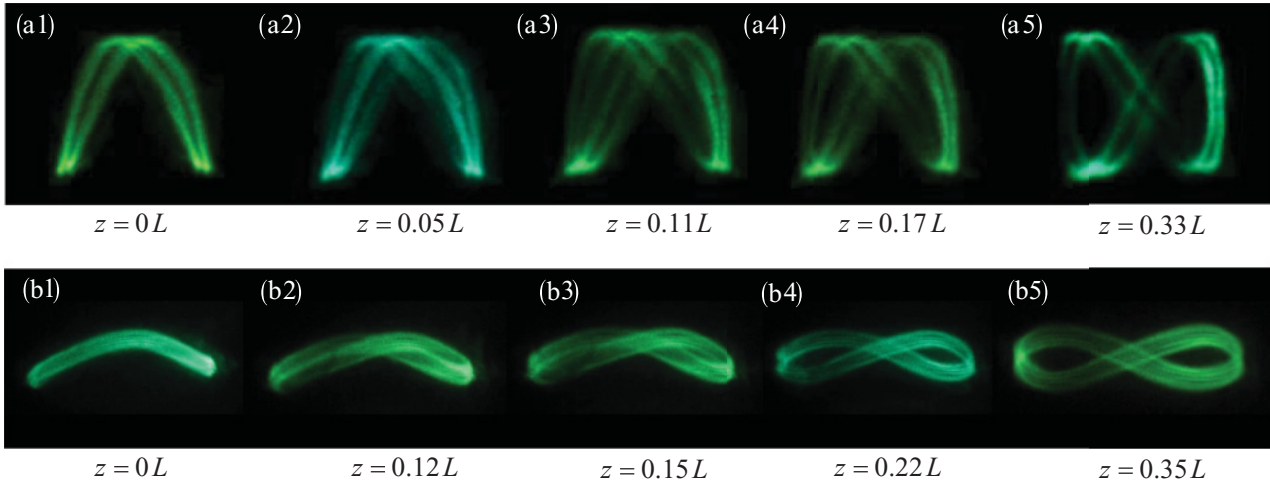


FIG. 8. (Color online) Experimental tomographic transverse patterns observed along the propagation direction from the beam waist. (a1)–(a5) $(\Delta x, \Delta y) = (0.21 \text{ mm}, 0.10 \text{ mm})$. (b1)–(b5) $(\Delta x, \Delta y) = (0.57 \text{ mm}, 0.10 \text{ mm})$.

cavities with a large off-axis tightly focused pumping spot of $\sim 25 \mu\text{m}$ are usually dominated by the 3D coherent waves with transverse patterns corresponding to single Lissajous figures. In this work we systematically find that the 3D coherent lasing waves can be manipulated by enlarging the pumping spot size to form more intricate transverse patterns corresponding to multiple Lissajous orbits as shown in the quantum eigenstates of the developed model. Figures 7(b)–7(c) depict the experimental observations for the cavity length L of 7.5 mm with the pumping size $\sim 50\text{--}100 \mu\text{m}$. It can be seen that the experimental observations agree very well with the numerical results in Figs. 1(b1)–1(b4), which is associated with our theoretical analysis that groups of eigenstates can be excited simultaneously to compose the corresponding Lissajous patterns. Note that the indices (p, q) are determined from the cavity length L and the degenerate conditions [12]. We verify that the number of Lissajous orbits in the lasing transverse pattern is governed by the spot size of the pumping beam. The larger the pumping size, the greater the number of Lissajous orbits that can be effectively excited.

In the preceding section, we demonstrated the effect of the parameter β which signifies the degree of coupling mechanism and governs the distribution of the states $|m_1 p, m_2 q\rangle_{\hat{H}_0}$ employed in the superposition of eigenstates $|n_1 p, n_2 q\rangle_{\hat{H}}$. In a laser resonator, the influence of β corresponds fairly to the amount of astigmatism arising from the off-axis pumping. While β is chosen, the parameter α can be realized as the Gouy phase shift [12,37], which differs along the propagation direction for Gaussian beams. As shown in Fig. 8, transverse patterns of different positions along the propagation direction are visibly consistent with the theoretical results in Fig. 3 for the evolution of HOs. Obviously, a three-dimensional evolutionary parametric surface can be exploited to interpret the transformation of the spatial patterns inside the cavity. The same clarification for single periodic Lissajous figures had been primarily provided [12] to show noticeable localization on the 3D parametric surface by observing the tomographic transverse patterns inside the cavities. Note that Figs. 8(a1)–8(a5), and Figs. 8(b1)–8(b5) are generated with off-axis pumping $(\Delta x, \Delta y) = (0.21 \text{ mm}, 0.10 \text{ mm})$, and

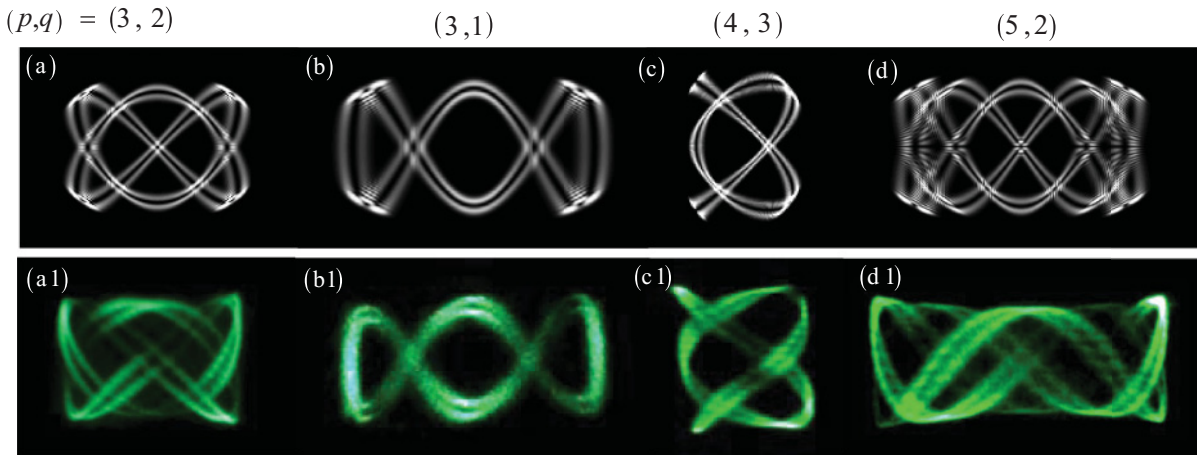


FIG. 9. (Color online) (a)–(d) Numerical wave patterns for the intensities of $|n_1 p, n_2 q\rangle_{\hat{H}}$ with different (p, q) . (a1)–(d1) Experimental results corresponded to the theoretical analysis. See the text for a detailed description of the parameters.

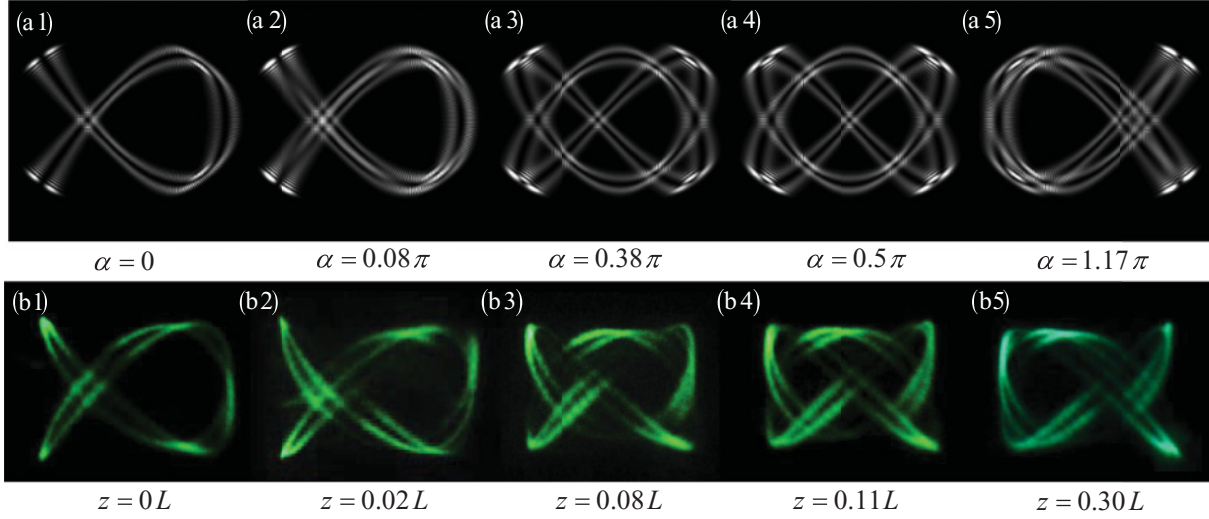


FIG. 10. (Color online) (a1)–(a5) Numerical wave patterns for the intensities of $|n_1 p, n_2 q\rangle_{\hat{H}}$ with $(p, q) = (3, 2)$ and varying α . (b1)–(b5) Experimental tomographic transverse patterns observed along the propagation direction from the beam waist for $(p, q) = (3, 2)$.

$(\Delta x, \Delta y) = (0.57 \text{ mm}, 0.10 \text{ mm})$, where $(\Delta x, \Delta y)$ are measured relative to the optical axis of the laser cavity and an objective lens is employed to reimage the near-field patterns on the screen.

In Figs. 9(a1)–9(d1), experimental observation of different (p, q) are displayed corresponding to numerical calculations of $|n_1 p, n_2 q\rangle_{\hat{H}}$, where $(p, q) = (3, 2)$, $(\alpha, \beta) = (\pi/2, \pi/2)$ for Fig. 9(a), $(p, q) = (3, 1)$, $(\alpha, \beta) = (\pi/2, \pi/2)$ for Fig. 9(b), $(\alpha, \beta) = (0, \pi/2)$, $(p, q) = (4, 3)$ for Fig. 9(c), and $(\alpha, \beta) = (\pi/2, \pi/2)$, $(p, q) = (5, 2)$ for Fig. 9(d), and all with $n_1 = 1$, and $N = 60$. Experimental results of the patterns $(p, q) = (3, 2)$, $(p, q) = (3, 1)$, $(p, q) = (4, 3)$, and $(p, q) = (5, 2)$, are observed at $L = 9.0 \text{ mm}$, $L = 4.9 \text{ mm}$, $L = 6.1 \text{ mm}$, and $L = 7.4 \text{ mm}$, respectively. In Figs. 10(a1)–10(a5), the transverse patterns along the propagation direction of $(p, q) = (3, 2)$ in Fig. 9(a1) are reconstructed agreeably, as depicted in Figs. 10(a1)–10(a5) for varying α . This agreement suggests that our quantum operator model of the coupled commensurate HO is applicable to the ubiquitous laser modes.

IV. CONCLUSION

In summary, we have systematically investigated the quantum signatures of the eigenstates corresponding to the coupled commensurate HO with $SU(2)$ coupling interactions. Furthermore, we have explored the analogous observation of the laser transverse modes from large-Fresnel-number degenerate cavities via varying pumping size. It has been experimentally verified that the 3D coherent lasing waves corresponding to the quantum states with multiple Lissajous orbits can be systematically generated by enlarging the pumping spot size. Finally, we employ the propagating property of the lasing modes to manifest the role of the phase factor introduced by the $SU(2)$ coupling interactions.

ACKNOWLEDGMENT

The authors acknowledge the National Science Council of Taiwan (NSCT) for their financial support of this research under Contract No. NSC-100-2628-M-009-001-MY3.

-
- [1] *Quantumlike Models and Coherent Effects*, edited by R. Fedele and P. K. Shukla (World Scientific, Singapore, 1995).
- [2] *New Perspectives in Physics of Mesoscopic Systems: Quantumlike Descriptions and Macroscopical Coherent Phenomena*, edited by S. De Martino, S. De Nicola, S. De Siena, R. Fedele, and G. Miele (World Scientific, Singapore, 1995).
- [3] D. Dragoman and M. Dragoman, *Quantum-Classical Analogies* (Springer, Berlin, 2004).
- [4] V. I. Karpman, *Nonlinear Waves in Dispersive Media* (Pergamon Press, Oxford, 1975).
- [5] G. P. Agrawal, *Nonlinear Fiber Optics* (Academic, San Diego, 1995).
- [6] M. A. Leontovich, *Izv. Akad. Nauk SSSR* **8**, 16 (1944).
- [7] M. A. Leontovich and V. A. Fock, *Zh. Éksp. Teor. Fiz.* **16**, 557 (1946).
- [8] D. Gloge and D. Marcuse, *J. Opt. Soc. Am. A* **59**, 1629 (1969).
- [9] R. Fedele, M. A. Man'ko, V. I. Man'ko, and V. G. Vaccaro, *Phys. Scr.* **68**, 377 (2003).
- [10] G. Nienhuis and L. Allen, *Phys. Rev. A* **48**, 656 (1993).
- [11] N. B. Rex, H. E. Tureci, H. G. L. Schwefel, R. K. Chang, and A. D. Stone, *Phys. Rev. Lett.* **88**, 094102 (2002).
- [12] Y. F. Chen, T. H. Lu, K. W. Su, and K. F. Huang, *Phys. Rev. Lett.* **96**, 213902 (2006).
- [13] K. F. Huang, Y. F. Chen, H. C. Lai, and Y. P. Lan, *Phys. Rev. Lett.* **89**, 224102 (2002).
- [14] T. Gensty, K. Becker, I. Fischer, W. Elsässer, C. Degen, P. Debernardi, and G. P. Bava, *Phys. Rev. Lett.* **94**, 233901 (2005).

- [15] Y. F. Chen, K. W. Su, T. H. Lu, and K. F. Huang, *Phys. Rev. Lett.* **96**, 033905 (2006).
- [16] R. Fedele and V. I. Man'ko, *Phys. Rev. E* **58**, 992 (1998).
- [17] R. Fedele and V. I. Man'ko, *Phys. Rev. E* **60**, 6042 (1999).
- [18] M. Moshinsky, *Phys. Rev.* **88**, 625 (1952).
- [19] S. Godoy, *Phys. Rev. A* **65**, 042111 (2002).
- [20] C. C. Chen, Y. T. Yu, Ross C. C. Chen, Y. J. Huang, K. W. Su, Y. F. Chen, and K. F. Huang, *Phys. Rev. Lett.* **102**, 044101 (2009).
- [21] O. Dippel, P. Schmelcher, and L. S. Cederbaum, *Phys. Rev. A* **49**, 4415 (1994).
- [22] P. K. Bhaduri, S. Li, K. Tanaka, and J. C. Waddington, *J. Phys. A* **27**, L553 (1994).
- [23] B. L. Johnson and G. Kirczenow, *Europhys. Lett.* **51**, 367 (2000).
- [24] S. G. Nilsson, *Mat. Fys. Medd. K. Dan. Vidensk. Selsk.* **29**, 16 (1955).
- [25] W. D. Heiss and R. G. Nazmitdinov, *Phys. Rev. Lett.* **73**, 1235 (1994).
- [26] R. G. Nazmitdinov, *Phys. Part. Nucl.* **40**, 71 (2009).
- [27] G. S. Agarwal and J. Banerji, *J. Phys. A* **39**, 11503 (2006).
- [28] Y. F. Chen, *Phys. Rev. A* **83**, 032124 (2011).
- [29] J. D. Louck, M. Moshinsky, and K. B. Wolf, *J. Math. Phys.* **14**, 692 (1973).
- [30] J. D. Louck, M. Moshinsky, and K. B. Wolf, *J. Math. Phys.* **14**, 692 (1973).
- [31] T. H. Lu, Y. C. Lin, H. C. Liang, Y. J. Huang, Y. F. Chen, and K. F. Huang, *Opt. Lett.* **35**, 345 (2010).
- [32] J. S. Schwinger and B. G. Englert, *Quantum Mechanics: Symbolism of Atomic Measurements* (Springer, Berlin, 2001).
- [33] J. J. Sakurai, *Modern Quantum Mechanics* (Addison-Wesley, Reading, MA, 1994).
- [34] M. S. Kumar and B. Dutta-Roy, *J. Phys. A* **41**, 075306 (2008).
- [35] A. Vaziri, G. Weihs, and A. Zeilinger, *J. Opt. B: Quantum Semiclassical Opt.* **4**, S47 (2002).
- [36] A. E. Siegman, *Lasers* (University Science, Mill Valley, CA, 1986).
- [37] T. D. Visser and E. Wolf, *Opt. Commun.* **283**, 3371 (2010).